AAS 08-278

HUBBLE SPACE TELESCOPE REDUCED-GYRO CONTROL LAW DESIGN, IMPLEMENTATION, AND ON-ORBIT PERFORMANCE

Brian R. Clapp[*], Patrick R. Ramsey[†], John H. Wirzburger[‡], Daniel C. Smith[§], and John C. Van Arsdall[**]

Following gyro failures in April 2001 and April 2003, HST Pointing Control System engineers designed reduced-gyro control laws to extend the spacecraft science mission. The Two-Gyro Science (TGS) and One-Gyro Science (OGS) control laws were designed and implemented using magnetometers, star trackers, and Fine Guidance Sensors in succession to control vehicle rate about the missing gyro axes. Both TGS and OGS have demonstrated on-orbit pointing stability of 7 milli-arcseconds or less, which depends upon the guide star magnitude used by the Fine Guidance Sensor. This paper describes the design, implementation, and on-orbit performance of the TGS and OGS control law fine-pointing modes using Fixed Head Star Trackers and Fine Guidance Sensors, after successfully achieving coarse-pointing control using magnetometers.

INTRODUCTION

The Hubble Space Telescope (HST) was launched into low Earth orbit on 24 April 1990 (STS-31) and has been serviced on-orbit by Space Shuttle crews four times since then. The fifth and final servicing, Servicing Mission 4 (SM4), is scheduled for October 2008. For the first fifteen years since launch, the science mission of the Hubble Space Telescope (HST) required using at least three rate gyros for attitude control. All six rate gyros were last replaced during HST Servicing Mission 3A (STS-103) in December 1999, but gyro failures in April 2001 and April 2003 prompted the NASA Goddard Space Flight Center (GSFC) to direct the HST Pointing Control System (PCS) engineers to design reduced-gyro control laws to extend the spacecraft science mission. Loss of the Space Shuttle Columbia in February 2003 appeared to end any future servicing of the HST; preservation of on-board resources became the focus of all efforts to maintain the HST as the premier orbital observatory for astronomical science. By February 2005, a two-gyro control law for the HST had been designed, implemented, and tested on-orbit, and this Two-Gyro Science (TGS) control system became the nominal science control system in August 2005, and it remains so today. Development of a One-Gyro Science (OGS) control law began in 2004, and HST science imaging performance with this control system was verified during on-orbit test in January 2008. Both TGS and OGS rely upon magnetometer control for large angle maneuvers and attitude control (with 10 deg or better accuracy) during Earth occultation of Fixed Head Star Trackers (FHSTs) and Fine Guidance Sensors (FGSs). FHST control dampens rates from the magnetometer mode, performs On-Board Attitude Determinations (OBADs) followed by maneuvers to remove residual attitude errors, and controls the HST

[*] Research Engineer Senior Staff, Lockheed Martin Corporation, Greenbelt, MD 20770 brian.clapp@lmco.com
[†] Research Engineer Senior, Lockheed Martin Corporation, Greenbelt, MD 20770 pramsey@hst.nasa.gov
[‡] Systems Engineer, Honeywell Technical Solutions, Inc., Greenbelt, MD 20770 jwirzburger@hst.nasa.gov
[§] Systems Engineering Manager, Lockheed Martin Corporation, Greenbelt, MD 20770 dsmith@hst.nasa.gov
[**] Senior Systems Engineer, Sagitta Solutions, Inc., Annapolis MD 21409 john@sagittasolutions.com

boresight pointing accuracy to within 55 arcseconds. Finally, FGS control dampens rates from the star tracker mode and acquires guide stars in Fine Lock to achieve pointing stability better than 7 milli-arcseconds for HST science imaging.

This paper describes the design, implementation, and on-orbit performance of the TGS and OGS fine-pointing modes using FHSTs and FGSs, after successfully achieving coarse-pointing control using the magnetometer mode. Design details are presented for the FHST and FGS modes, including estimation of HST vehicle rates using sensor-computed star vectors, linear stability analyses for the control laws, non-linear time domain simulation predictions, and how those predictions compare with in-flight performance. Sequences are presented showing the steps required to transition from low pointing accuracy (several degrees) to the high accuracy (several milli-arcseconds) required for HST science.

HST POINTING CONTROL SYSTEM OVERVIEW

The hardware complement of the HST PCS requires a broad dynamic range in order to maneuver from target-to-target and achieve the required 7 milli-arcsecond (mas) pointing stability during science imaging. The primary PCS is a 3-axis stabilized zero-momentum attitude determination and control system designed using components dating from the late 1970's.[1,2] Pointing control actuation is achieved using four Reaction Wheel Assemblies (RWAs) and four Magnetic Torquer Assemblies for RWA speed management. The primary PCS sensors consist of six rate integrating gyros, three FGSs, three NASA Standard FHSTs, and two Magnetic Sensing Systems (MSSs), or magnetometers.

Although HST science instruments have been upgraded during servicing using state-of-the-art detectors and optics, the PCS hardware complement is very similar to the original-design components used at launch. Minor hardware modifications have been made to the orbital-replacement rate gyros to increase longevity. FGS orbital replacements have also been slightly revised to increase the dynamic range of the interferometric Fine Error Signal (FES), or S-curve, compared to the three units originally launched on-board the HST.[3] Neither of these hardware changes was made with the intent of changing HST pointing performance relative to the original PCS design.

The HST baseline control system at launch used a Proportional Integral Derivative (PID) classical control law accompanied by an attitude observer to estimate rate gyro biases.[1,2] These control algorithms were significantly modified in the on-board flight computer within the first two years after launch to attenuate jitter induced by solar array vibration.[4] Successful rejection of solar array disturbances was achieved by increasing the control law closed-loop bandwidth from 1.3 Hz to 2.2 Hz and by providing additional gain at solar array fundamental modes measured on-orbit at 0.1 Hz and 0.67 Hz.[5] After these control law changes were implemented, HST science performance finally realized the 7 mas pointing stability requirement during extended observation intervals. The most significant hardware improvement affecting HST pointing occurred after Servicing Mission 3B (STS-109) in March 2002 when the original bi-stem style flexible solar arrays (SA1 and SA2 design) were replaced with the rigid Solar Array 3 (SA3) design. SA3 eliminated the solar array vibration problem and allowed the baseline pointing control law to be used again.

A brief description of the HST PCS operational scenario under 3-gyro control follows to allow comparison with the new reduced-gyro scenarios presented later. HST maneuvers target-to-target using RWAs while sensing attitude using at least three rate gyros in high-rate mode. Gyro scale factors are calibrated to ensure that post-maneuver errors are less than 300 arcseconds (asec). Rate gyros autonomously switch to high-precision low-rate mode when command generator rates fall below 9 asec/sec. Scheduled attitude updates are performed using off-boresight FHSTs to reduce attitude errors to less than 55 asec prior to starting the guide star acquisition process with either one or two FGSs. FHSTs need to track stars for only one minute to successfully perform an attitude update. An FGS Field of View (FOV) lies between 10.2-14.0 arcminutes away from the telescope boresight; consequently, science observations lasting more than 5-minutes typically use two FGSs, enabling roll error control. The FGS guide star acquisition process then begins with first the primary FGS then the secondary FGS acquiring planned guide stars within the (5 asec x 5 asec) FGS Instantaneous Field of View (IFOV).[6] Each FGS is autonomously commanded by a Fine Guidance Electronics (FGE) computer to transition through Search mode, Coarse Track mode, and finally Fine Lock mode to achieve 2-axis interferometer lock on its guide

star. After successfully acquiring guide stars, the spacecraft flight computer performs error checks, commands the RWAs to perform fine error correction maneuvers, activates the attitude observer, and transitions the observatory to science mode once the attitude observer has settled. HST science observations include both fixed and moving target exposures of varying duration.

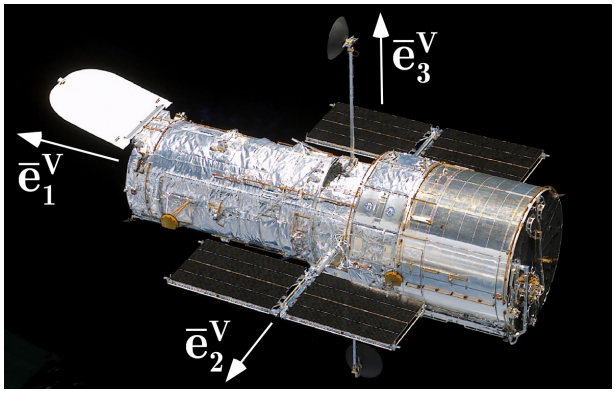

Figure 1 HST Vehicle Frame Axis Convention

Using the baseline 3-gyro control law, the PCS relies primarily upon the low-noise rate gyros for attitude error correction at a 40 Hz sample rate. The six HST rate gyros are not oriented along the spacecraft vehicle axes, as shown in Figure 1. Gyro input axis unit vectors relative to the HST vehicle frame are shown in Table 1 in accordance with Eq. (1)[*]. The full capabilities of the FGSs were not utilized in the baseline 3-gyro control law design, likely due to skepticism by the original PCS designers that the FGSs would function correctly on-orbit. FGS Star Selector Servo (SSS) angles and Photomultiplier Tube (PMT) counts, received by the HST flight computer at a 40 Hz sample rate, were used to compute FGS attitude errors using linearized equations. The FGS attitude errors were then averaged over 40-samples and input to the attitude observer at a 1 Hz rate for on-board gyro bias estimation. Because the FGS was used for low-rate attitude error measurement in the baseline 3-gyro control law, the linearized FGS attitude error equations were sufficient, and implementing the non-linear spherical trigonometric star vector equations was avoided in the original DF-224 flight computer, having limited processing power.

$$\bar{g}^V = g_1^V \bar{e}_1^V + g_2^V \bar{e}_2^V + g_3^V \bar{e}_3^V \tag{1}$$

Table 1 Rate Gyro Input Axis Unit Vector Orientation in HST Vehicle Frame

Gyro Number	g_1^V	g_2^V	g_3^V
1	-0.52547	0	-0.85081
2	-0.52547	0	0.85081
3	-0.58566	-0.61716	-0.52547
4	0.58566	0.61716	-0.52547
5	-0.58566	0.61716	-0.52547
6	0.58566	-0.61716	-0.52547

Typical HST pointing stability using the baseline 3-gyro control law is shown in Table 2 for all 3-gyro combinations used on-orbit, to date. Pointing performance varies substantially depending upon the gyro combination used, due to gyro input axis sensitivity to boresight motion, but all combinations meet the 7 mas pointing stability requirement.

[*] Vector and tensor nomenclature used throughout this paper is described at the end of the paper in Table 10.

Table 2 HST On-Orbit Pointing Stability using Baseline 3-Gyro Control Law

Gyro Combination	Boresight Jitter (mas, 60-sec RMS, 1-σ)
1-2-4	3.69
1-2-5	3.77
1-3-5	5.40
2-3-4	6.31
2-3-5	1.93
3-4-5	2.89
3-5-6	3.06

CHARACTERISTICS OF HST FIXED HEAD STAR TRACKERS

The FHSTs are NASA Standard 1970's vintage star trackers manufactured by Ball Brothers.[7] They employ an electronic search and track technique using an analog image dissector tube and a photomultiplier detector along with supporting electronics. The FHSTs have an 8° x 8° FOV and are capable of acquiring and tracking stars between 2.0-6.5 magnitude visual (mv). The trackers provide digital horizontal and vertical star position output to the HST flight computer at a 10 Hz sample rate. The FHST noise equivalent angle is 16 asec RSS. Unlike modern star trackers, the FHSTs have no internal processing to output attitude quaternions, and attitude errors from the FHSTs are computed on-board the HST flight computer. The boresight unit vector components in the HST vehicle frame for each of the three FHSTs are shown in Table 3.

Table 3 FHST Boresight Axis Unit Vector Orientation in HST Vehicle Frame

FHST Number	t_1^V	t_2^V	t_3^V
1	0	0	-1
2	-0.6547	-0.3779	-0.6546
3	-0.6547	0.3779	-0.6546

The FHSTs exhibit a number of unfortunate characteristics that complicate their use as a control sensor over extended periods of time. Some known features of the FHSTs are the ability to lock and track non-stellar objects, such as satellites and planets, difficulty tracking double stars, and an inability to avoid very bright stars. Because the FHSTs have no internal processing available to detect these unwanted light sources, development of algorithms in the HST flight computer was necessary to increase FHST data quality. The high relative motion of satellite and planet tracking results in erroneous measurement of HST position. When double stars do not have adequate separation for the FHST to discriminate between the light sources, the FHST scan tends to drift between the sources, occasionally exhibiting large single-sample changes in horizontal and vertical position measurements. Some light sources are so bright that the FHST scan cannot achieve a stable star presence, and the scan jump associated with a FHST Break Track is insufficiently sized for the scan to be moved sufficiently far away from the bright source, resulting in the scan being stuck in a region of the FHST FOV. These have been referred to as Stuck On Bottom events due to the tendency of the FHST scan to be limited to the bottom third of the vertical scan for extended durations. A few events have occurred in different regions of the FOV, but most occur near the bottom of the FHST FOV.

CHARACTERISTICS OF HST FINE GUIDANCE SENSORS

The three FGSs on-board the HST are used for fine guiding and for astrometry science. They were built by Perkin Elmer. When used for fine guiding, the FGSs are capable of acquiring and maintaining interferometer lock on guide stars with brightness ranging between 9.0-14.5 mv with a noise equivalent angle of 2 mas RSS. Within each FGS are two Star Selector Servo units (SSS-A and SSS-B) that rotate optical components to direct the star image onto beam splitters and Koester prisms to reach the four PMTs.[3] The angular positions of the SSSs determine which 5 asec x 5 asec region (the IFOV) of the overall FOV

enters the field stops of the PMTs. The interferometric FES, the S-curve computed from PMT measurement, senses 2-axis tilt of the star image beam that is used at 40 Hz by the FGE Control Law to command the SSSs to center the star image upon the Koester prisms, thus achieving Fine Lock on the target star. The target star position in 2-axes is computed from SSS angles and PMT counts by the spacecraft flight computer. The FGE Control Law also receives feed-forward commands from the flight computer that allows the HST to track moving targets while retaining lock on the same pair of FGS guide stars. The majority of the FGE Control Law resides in firmware, but many parameters (called K-Factors), such as gains, limiters, and other operational values, can be uplinked from the ground. The SSS units are complete servo mechanisms, built by Baldwin Electronics Inc., containing ball bearing pairs, an optical shaft encoder, a brushless DC motor, and analog electronics including a control law with a bandwidth of approximately 8 Hz. Unit vector components at the center of the FGS FOV in the HST vehicle frame are shown in Table 4.

Table 4 FGS FOV-Center Unit Vector Orientation in HST Vehicle Frame

FGS Number	f_1^V	f_2^V	f_3^V
1	0.9999938	0.0035197	0
2	0.9999938	0	-0.0035197
3	0.9999938	-0.0035197	0

Two of the three original FGSs have been replaced since launch, FGS-1 in February 1997 during Servicing Mission 2 (STS-82), and FGS-2 in December 1999 during Servicing Mission 3A (STS-103), as shown in Figure 2. Replacement of these units was necessary because of SSS bearing and lubricant degradation that was caused by excessive use of Coarse Track mode during early-mission science imaging.

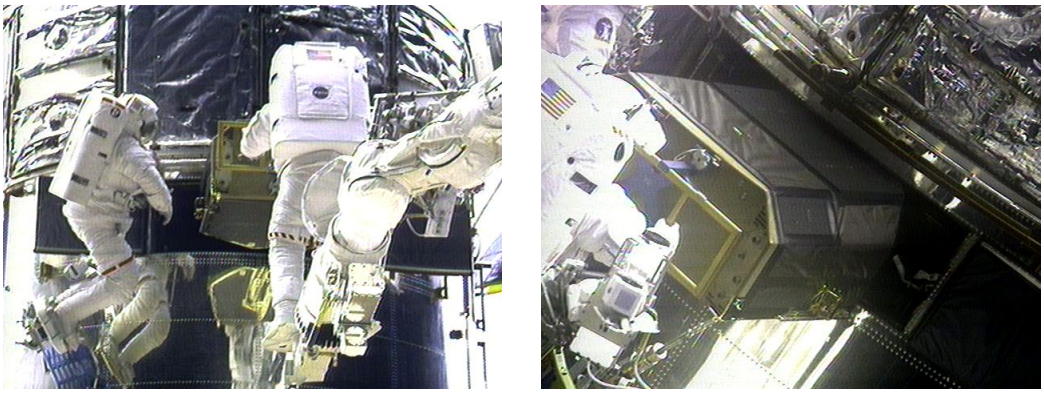

Figure 2 Replacement of FGS-2 during HST Servicing Mission 3A

FGE Coarse Track Mode is part of the normal guide star acquisition process, after the SSSs have completed a Spiral Scan in FGE Search Mode to detect Star Presence in the IFOV. During Coarse Track, the FGE commands the SSSs to sinusoidally dither ±0.39° in shaft angle, resulting in a circular nutation of the FGS IFOV with a diameter of roughly 5.2 asec around the target star. Each nutation takes 1-sec to complete. During Coarse Track nutation, the 40 Hz FGE Control Law actively controls the center of nutation by balancing all four PMT measurements. Under 3-gyro control, 10-12 sec of Coarse Track was needed to locate the target star light centroid. Upon completing Coarse Track, the FGE initiates Fine Lock Mode that starts by open-loop commanding the SSSs to move the IFOV to the Fine Lock Backoff position, approximately 400 mas from the Coarse Track nutation center. The FGE then open-loop commands the SSSs to perform the Fine Lock Walkdown, a diagonal stepping of the IFOV towards the expected target star position. Under 3-gyro control, HST rates are stable during the Fine Lock Walkdown, while the primary FGS scan steps to locate the target star. At the end of the Fine Lock Walkdown, Fine Lock Data Valid is declared when FGS PMTs in both axes sense the interferometric S-curve. The FGE Control Law

maintains Fine Lock by controlling the SSSs to center the target star image on the Koester prisms, and the FGE signals the flight computer to begin using the FGS in the PCS to attenuate attitude errors in preparation for science imaging.

DEVELOPMENT OF REDUCED-GYRO SCIENCE MODES

HST reduced-gyro modes were designed and implemented using MSSs, FHSTs, and FGSs to control vehicle rate about the missing gyro axes. TGS and OGS each contain three control modes, and acronyms for each pointing control mode are listed in Table 5. Figure 3 illustrates the operational interaction between these modes that was developed for TGS and OGS.

Table 5 Reduced-Gyro Pointing Control Mode Acronyms

Attitude Sensor	Sensor Acronym	Pointing Control Mode Acronym		
		Generic (TGS or OGS)	Two-Gyro Science (TGS)	One-Gyro Science (OGS)
Magnetometer	MSS	MxG	M2G	M1G
Fixed Head Star Tracker	FHST	TxG	T2G	T1G
Fine Guidance Sensor	FGS	FxG	F2G	F1G

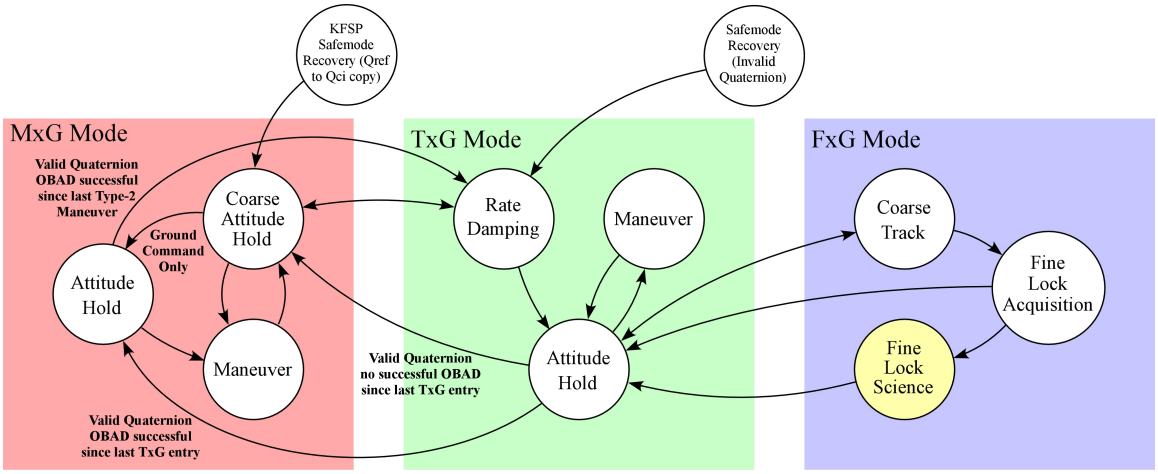

Figure 3 Reduced-Gyro Science Mode Transition Diagram

The remainder of this paper focuses upon the star-sensing reduced-gyro modes, TxG and FxG. These modes are similar in that the alignment in the HST vehicle frame of the missing gyro axes is fixed relative to the star sensor boresight. In contrast, the design of the MxG modes was complex due to the motion of the earth magnetic field vector in the HST vehicle frame. The MxG concept is based upon computing the difference between the MSS-measured magnetic field and an on-board magnetic field model to compute attitude and rate errors for control of the missing gyro axes.[8] Slow-moving magnetic fields and alignment of the magnetic field vector with the missing gyro axes results in MxG errors of up to 10 deg under worst-case conditions. However, HST attitude and rate errors under MxG control are low enough to allow FHSTs to acquire and track stars, damp MxG rates, and perform OBAD correction maneuvers so that fine pointing may be achieved.

TWO-GYRO SCIENCE

TGS was the first new science mode developed for the HST since launch. Every engineering discipline within the HST program at GSFC was involved in the design of TGS, and major changes in the science mission scheduling system, at the Space Telescope Science Institute (STScI) at Johns Hopkins University in Baltimore, were needed to accommodate the new mode.[9] TGS was challenging to design for several reasons, but the primary reason was due to errors anticipated during M2G. Under 3-gyro control, attitude

errors typically never exceeded 30 arcminutes, but with TGS, attitude errors of up to 10 deg were expected on occasion. This affected the function of not only pointing control and flight software subsystems, but also communications, power, and safing subsystems. Another challenge facing the engineering design teams was the development of new operational scenarios needed for TGS, as shown in Figure 3. The residual M2G errors were larger than the error correction capability for the 3-gyro type of FHST attitude updates performed prior to guide star acquisitions; therefore, an OBAD scheme previously used in the ground station software had to be implemented in the HST flight computer as part of the TGS effort. After the T2G controller dampens residual M2G rates, an OBAD (using 2 FHSTs in map mode) and maneuver combination during T2G control measures and corrects residual M2G attitude errors. TGS challenged mission schedulers at the STScI to fit science proposals within new operational constraints, such as the required overlap of FHST and FGS visibility during T2G-to-F2G mode transitions, without significantly degrading HST science efficiency. The TGS feasibility study began in May 2003, and TGS was successfully demonstrated during On-Orbit Test (OOT) in February 2005 using Gyros 2 and 4 in the control system. TGS was entered permanently as the default HST science control system on August 29, 2005 using Gyros 1 and 2 in the PCS. Gyro 4 was turned-off shortly thereafter.

Orthogonal Gyro Frame for Two-Gyro Science

An Orthogonal Gyro Frame (OGF) and a Non-Orthogonal Gyro Frame are defined for TGS, and transformation matrices are developed between these reference frames and the HST vehicle frame. The input axes of the two gyros used for TGS, Gyro-A and Gyro-B, form a plane, called the Gyro Plane, as shown in Figure 4. Any two HST gyro input axes are not orthogonal to each other (as indicated in Table 1).

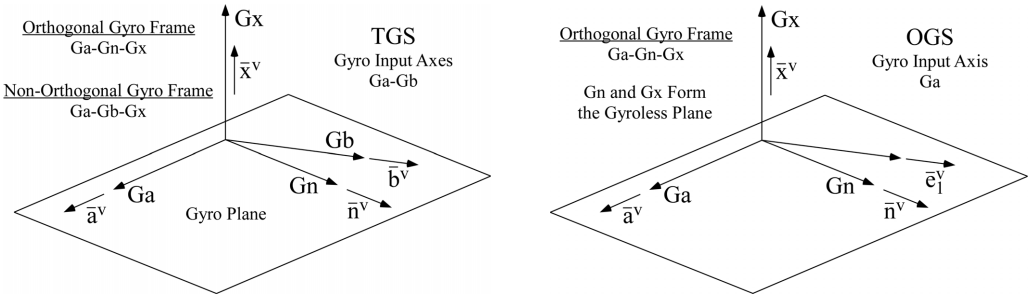

Figure 4 TGS and OGS Orthogonal Gyro Frames

The input axis unit vectors for Gyros A and B are shown in Eq. (2), the Ga-axis and Gb-axis, respectively. The unit vector normal, Eq. (3), is along the Gx-axis, or the missing-gyro axis. These three non-orthogonal unit vectors define the Two-Gyro Frame.

$$\bar{a}^V = a_1^V \bar{e}_1^V + a_2^V \bar{e}_2^V + a_3^V \bar{e}_3^V \qquad \bar{b}^V = b_1^V \bar{e}_1^V + b_2^V \bar{e}_2^V + b_3^V \bar{e}_3^V \tag{2}$$

$$\bar{x}^V = x_1^V \bar{e}_1^V + x_2^V \bar{e}_2^V + x_3^V \bar{e}_3^V = \left(\bar{a}^V \times \bar{b}^V\right) \Big/ \left\| \bar{a}^V \times \bar{b}^V \right\| \tag{3}$$

The Orthogonal Gyro Frame for TGS is completed by forming the Gyro Plane Gn-axis unit vector given by Eq. (4). Transformation matrices between the vehicle frame and the non-orthogonal Two-Gyro Frame and between the vehicle frame and the OGF are constructed in Eq. (5). The T2G and F2G control laws implemented in the HST flight computer are coordinatized in the OGF.

$$\bar{n}^V = n_1^V \bar{e}_1^V + n_2^V \bar{e}_2^V + n_3^V \bar{e}_3^V = \bar{x}^V \times \bar{a}^V \tag{4}$$

$$T_{\alpha\beta}^{GV} = \begin{bmatrix} a_1^V & a_2^V & a_3^V \\ b_1^V & b_2^V & b_3^V \\ x_1^V & x_2^V & x_3^V \end{bmatrix} \qquad T_{\alpha\beta}^{OV} = \begin{bmatrix} a_1^V & a_2^V & a_3^V \\ n_1^V & n_2^V & n_3^V \\ x_1^V & x_2^V & x_3^V \end{bmatrix} \tag{5}$$

Table 6 Angles between Gx-Axis and HST and FHST Boresights for Gyro Combinations in TGS

Gyro-A	Gyro-B	FHST	Gx (V1-Axis)	Gx (V2-Axis)	Gx (V3-Axis)	Angle (degrees) from V2-Axis to Line of Intersection of Gyro-Plane and V2-V3 Plane (Jitter Ellipse Gx-Axis)	Angle Between Gx and V1 (degrees)	Angle Between Gx and FHST Boresight (degrees)
1	2	1	0.000	1.000	0.000	90.000	90.000 #	90.000 &
1	2	2	0.000	1.000	0.000	90.000	90.000 #	67.795
1	2	3	0.000	1.000	0.000	90.000	90.000 #	67.795
1	4	1	0.530	-0.782	-0.328	112.723	57.977	70.883
1	4	2	0.530	-0.782	-0.328	112.723	57.977	80.634
1	4	3	0.530	-0.782	-0.328	112.723	57.977	64.637
1	6	1	-0.530	-0.782	0.328	67.278	57.977	70.883
1	6	2	-0.530	-0.782	0.328	67.278	57.977	64.637
1	6	3	-0.530	-0.782	0.328	67.278	57.977	80.634
2	4	1	-0.801	0.339	-0.494	34.414	36.820 *	60.369
2	4	2	-0.801	0.339	-0.494	34.414	36.820 *	43.965
2	4	3	-0.801	0.339	-0.494	34.414	36.820 *	12.637 +
2	6	1	0.801	0.339	0.494	145.586	36.820 *	60.369
2	6	2	0.801	0.339	0.494	145.586	36.820 *	12.637 +
2	6	3	0.801	0.339	0.494	145.586	36.820 *	43.965
4	6	1	-0.668	0.000	-0.744	0.000	48.101	41.899
4	6	2	-0.668	0.000	-0.744	0.000	48.101	22.411
4	6	3	-0.668	0.000	-0.744	0.000	48.101	22.411

Best F2G | * Worst F2G | & Best T2G | + Worst T2G

A qualitative measure of TGS pointing performance is estimated by considering the angle between the Gx-axis and the FHST or FGS boresight axis. When the angle is small, for example with Gyros 2 and 4 and FHST 3 as shown in Table 6, the star sensor poorly measures vehicle rates about the missing gyro axis. Not all two-gyro combinations are listed in Table 6; Gyros 3 and 5 had already failed by the time TGS was developed, and they are not listed. The input axes of all six gyros have significant components in the roll axis ($\overline{e}_1^V$) which is nearly the FGS boresight axis. Therefore it was anticipated that HST science imaging performance in Fine Lock would not be degraded by poor gyro-to-FGS alignment in TGS.

Rate Estimation for Star Sensing Modes in Two-Gyro Science

Optimal Gx-axis rate estimation for T2G and F2G modes is evaluated by performing parameter optimization given two non-orthogonal gyro rate measurements, ω_1^G and ω_2^G, along with a star sensor unit vector measurement, $\overline{s}^V$, in either the FHST or FGS boresight direction. The total derivative of the star vector in the HST vehicle frame is given by Eq. (6) after introducing a nominally zero error vector, $\overline{\lambda}^V$, and inserting expressions found in Eq. (7). Minimizing the cost function, J, in Eq. (8) with respect to the unknown Gx-axis vehicle rate, ω_3^G, results in the TGS rate estimation equation, Eq. (9).

$$\overset{o}{\overline{s}}{}^V = \dot{\overline{s}}^V + \overline{\omega}^V \times \overline{s}^V \qquad \overline{\lambda}^V = \overset{o}{\overline{s}}{}^V - \dot{\overline{s}}^V + \overline{\overline{P}}^{VG} \bullet \overline{\omega}^G \tag{6}$$

$$\overline{\overline{P}}^{VG} = \overline{\overline{\tilde{s}}}^V \bullet \left(\overline{\overline{T}}^{GV} \right)^{-1} \qquad \overline{\overline{\tilde{s}}}^V = \overline{e}_\alpha^V \tilde{s}_{\alpha\beta}^V \overline{e}_\beta^V, \quad \tilde{s}_{\alpha\beta}^V = \begin{bmatrix} 0 & -s_3^V & s_2^V \\ s_3^V & 0 & -s_1^V \\ -s_2^V & s_1^V & 0 \end{bmatrix} \tag{7}$$

$$\frac{\partial J}{\partial \omega_3^G} = 0 \qquad J = \sum_{\alpha=1}^{3} \left(\lambda_\alpha^V \right)^2 \tag{8}$$

$$\omega_3^G = \left[\sum_{\alpha=1}^{3} \left(\dot{s}_\alpha^V - \overset{o}{s}{}_\alpha^V - P_{\alpha 1}^{VG} \omega_1^G - P_{\alpha 2}^{VG} \omega_2^G \right) P_{\alpha 3}^{VG} \right] \Bigg/ \left[\sum_{\alpha=1}^{3} \left(P_{\alpha 3}^{VG} \right)^2 \right] \tag{9}$$

The total derivative of the star vector, $\overset{o}{\overline{s}}{}^V$, is computed in the HST flight computer as the cross product of the rate of change of velocity aberration with the star vector, $\overline{s}^V$. The star vector derivative, $\dot{\overline{s}}^V$, is computed by back-differencing star vector present and past values. To ensure that this derivative is

orthogonal to the star vector, the average of star vector present and past values is used in Eq. (7). FHST and FGS star vector equations used for TxG and FxG are shown later.

TGS Operational Flow from T2G through F2G

The high-level mode transition diagram shown in Figure 3 broadly shows how the various TGS modes interact, but it hides many of the sensor-level details inherent to the design. Flow diagrams for T2G in Figure 5 and F2G in Figure 6 illustrate the intra-modal operation of these control modes to allow transition from M2G to milli-arcsecond pointing accuracy required for science in F2G.

The T2G control mode performs three functions, Rate Damping, Maneuver, and Attitude Hold, using three gain sets to control the Gx-axis, as shown in Figure 5. Rate control in T2G requires only a single FHST to track stars and damp M2G rates, but a second FHST is required to produce sufficiently accurate OBAD solutions followed by maneuvers to correct M2G-induced attitude errors. While performing the OBAD, rate control tracker switching is performed to allow star mapping with more than one FHST. After correcting FHST-measured attitude errors, the T2G Attitude Hold submode maintains control of Gx-axis attitude and rate through the start of the FGS guide star acquisition process until the primary FGS assumes rate control authority.

Early TGS designs assumed maximizing time in T2G was preferable to M2G control, due to the errors anticipated while controlling with the MSS while the FGS is occulted. However, TGS flight experience demonstrated that the opposite was true. STScI science scheduling successfully mitigated magnetic field alignments with the Gx-axis, and M2G attitude errors rarely exceeded 4 deg. At the same time, maximizing the time spent in T2G provided additional opportunity for the FHSTs to track non-stellar objects, which resulted in a substantial number of failed FGS guide star acquisitions. TGS currently reverses this control mode preference by maximizing time in M2G and reducing time in T2G to the minimum necessary to bridge the M2G and F2G control modes.

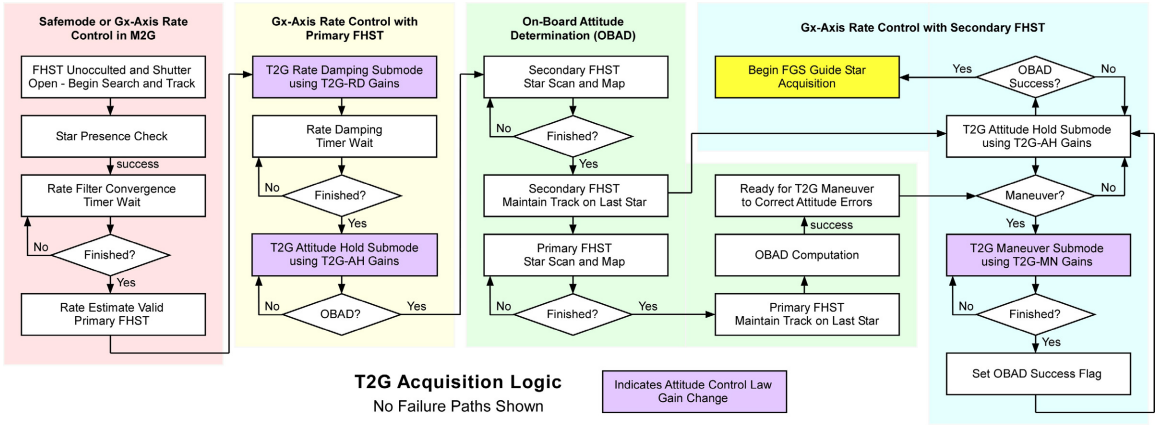

Figure 5 FHST Acquisition Process in TGS

F2G has a complex operational flow primarily because the FGS is capable of sensing attitude errors over a large dynamic range (0.002 asec - 55 asec). During the TGS guide star acquisition process, shown in Figure 6, F2G uses three different sets of control law gains for damping vehicle rates and trimming attitude errors. Similar to the baseline 3-gyro control mode, either one or two FGSs are required to complete the guide star acquisition process, depending upon science image duration and the need for roll attitude control by the FGSs. While the Gx-axis rate is controlled by a FHST in T2G, the primary FGS acquires and tracks its guide star in Coarse Track. F2G-CT gains are activated in the PCS, and Gx-rate control dampens T2G rates over 20 sec. After timer expiration, F2G-CT control of Gx-axis rates terminates, and the primary FGS proceeds with the Fine Lock Walkdown during open-loop control of Gx-axis rate. The open-loop interval is typically no more than 8-10 sec. After the primary FGS acquires its guide star in Fine Lock, the HST flight computer closes the Gx-axis rate loop and controls the Gx-axis using the primary FGS using the F2G-FL controller. If a second FGS is required for the science

observation, the secondary FGS guide star acquisition completes. Once both FGSs are successfully in Fine Lock, a sequence of attitude error corrections and observer configuration occurs prior to initializing the vehicle and control law for science. During the acquisition process, the primary FGS remains in Coarse Track for approximately 29 sec.

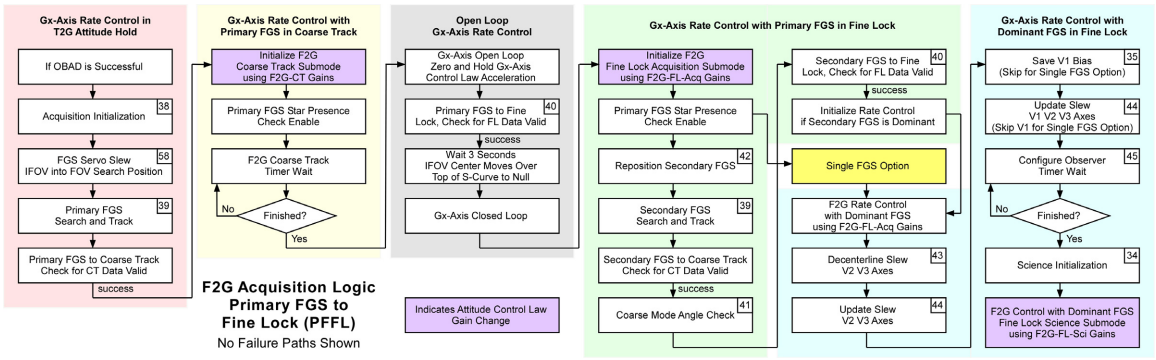

Figure 6 FGS Guide Star Acquisition Process in TGS

TRACKER AND TWO-GYRO CONTROL MODE (T2G)

The T2G control system was intentionally designed to maximize the use of existing flight software code in order to streamline development, so it is similar to the HST baseline 3-gyro control system. The green-shaded boxes in Figure 7 show the flight software changes required to implement T2G relative to the 3-gyro control system. The new additions to the 486 Flight Software include transformations required to coordinatize the T2G Control Law in the OGF, star vector and T2G rate estimation processing in the T2G feedback path, and Butterworth filters to reduce FHST noise.

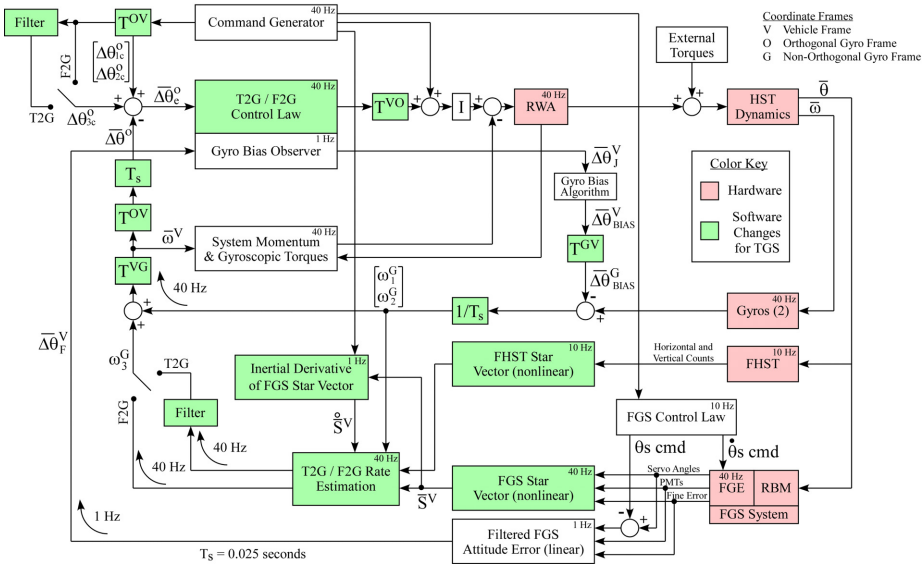

Figure 7 T2G and F2G Control System Block Diagram

The T2G design concept estimates the Gyro Plane normal-component of vehicle rate, ω_3^G, at 40 Hz from the 10 Hz FHST star vector and 2-gyro measurement, combines this with Gyro Plane rate measurements ω_1^G and ω_2^G, transforms the resulting rate vector into the OGF, and uses this feedback input

to the attitude control law as though it originated from three rate gyros. The T2G control laws are the first to use the FHST as a rate control sensor for the HST.

T2G Design

The three T2G submodes, Rate Damping, Maneuver, and Attitude Hold, all use a classical PID controller structure. These controllers operate at 40 Hz, with the FHST star vector provided at 10 Hz due to FHST hardware limitations. The Rate Damping T2G controller was designed to quickly reduce the relatively high vehicle rates from M2G control; therefore, it was designed with a high position gain and bandwidth compared to the other T2G submodes. After damping Gx-axis rates, position gain and bandwidth are reduced in the Attitude Hold and Maneuver submodes to reduce position and rate noise during the OBADs, attitude correction maneuvers, and the beginning of the FGS guide star acquisition process. Note that steady state position error was not a concern for the Rate Damping submode so integral gain is not used, effectively making the T2G Rate Damping controller a PD controller.

The star unit vector in the FHST frame is computed from tracker horizontal and vertical counts, H and V, respectively, as shown in Eq. (10). The FHST star vector is corrected for optical distortion and misalignment and then transformed into the HST vehicle frame prior to use in Eq. (9), the Gx-axis rate estimation equation. The total derivative of the star vector, $\frac{o}{s}^{V}$, in the Gx-axis rate estimation equation, is small relative to the FHST accuracy, and this term is not used for TxG.

$$\bar{s}^{T} = \begin{bmatrix} \tau \\ -\tau \tan\theta \\ \tau \tan\varphi \end{bmatrix} \qquad \begin{aligned} \tau &= \left(1 + \tan^2\varphi + \tan^2\theta\right)^{-1/2} \\ \varphi &= kH, \quad k = 3.6285\left(10^{-5}\right)\text{rad/count} \\ \theta &= kV, \quad k = 3.6285\left(10^{-5}\right)\text{rad/count} \end{aligned} \tag{10}$$

The Gx-axis rate estimate for T2G requires additional filtering prior to input into the control law due to the relatively noisy FHST star position data from which the estimate is derived. A 0.1 Hz low-pass Butterworth filter at the rate estimate output provides adequate attenuation of high frequency sensor noise without introducing excessive lag. An identical filter was also inserted at the command generator Gx-axis rate output to provide a matching lag to minimize transient attitude errors during maneuvers.

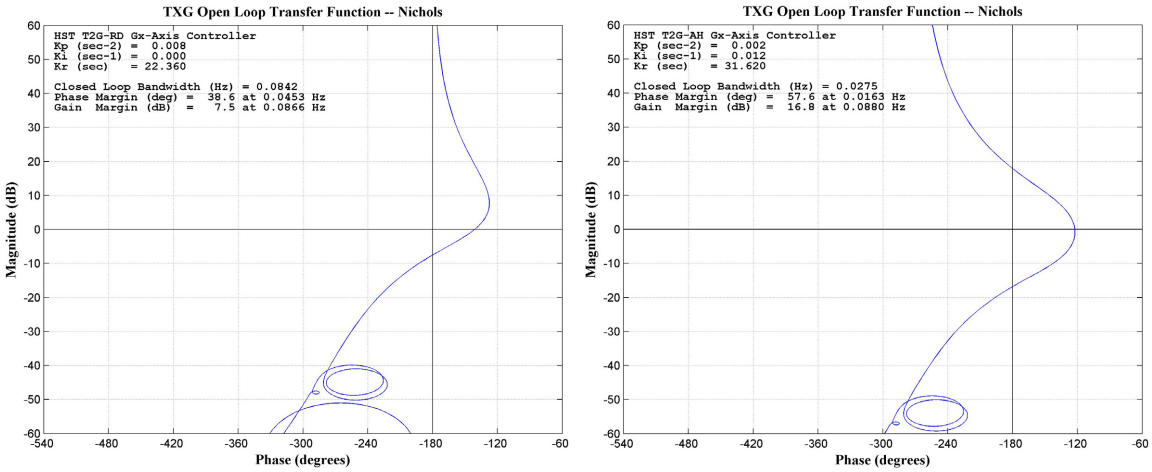

Figure 8 T2G Rate Damping and Attitude Hold Control Law Nichols Plots for the Gx-Axis

T2G stability analysis plots are shown in Figure 8 for the T2G Rate Damping and Attitude Hold submodes. T2G maneuver gains are identical to the Attitude Hold gain set. These are single-axis linear open-loop transfer function plots for the Gx-axis while using the FHST as a rate sensor. The T2G controller bandwidth is below the HST structural mode frequencies, as shown in Figure 8. The Rate Damping control law has a higher closed-loop bandwidth (0.084 Hz) compared to the Maneuver and

Attitude Hold control laws (0.028 Hz). The Nichols plots demonstrate that the T2G Gx-axis controllers have adequate stability margins; the gain and phase margins are written on the figures. Nichols plots for the T2G Gyro Plane axes are identical to the 3-gyro PD-gain Nichols plots, which are also the same as the Nichols plots for the F2G-CT Gyro Plane axes, shown later in Figure 11. Single-axis stability analysis is sufficient for HST because there is insignificant coupling between OGF axes in T2G mode.

Performance of the T2G controllers was predicted using the PCS high fidelity non-linear time domain simulation, HSTSIM. PCS engineers evaluated T2G rate damping time, position error following vehicle maneuvers, and position and rate errors during extended periods of Attitude Hold. All FHST and gyro pair combinations, listed in Table 6, were simulated to bound worst-case T2G performance. Performance of the Rate Damping submode was simulated using twice the predicted worst-case vehicle rate during M2G control (0.06 deg/sec), and the greatest time required to reduce HST rates below 2 asec/sec was 107 sec (120 sec required). Performance of the T2G Maneuver submode was evaluated by simulating 15°, 2°, and 0.5° maneuvers, and the predicted worst-case post-maneuver errors were 41 asec, 16 asec, and 15 asec, respectively. It takes the HST 96 minutes to complete an orbit, so T2G performance simulated over 60-minute intervals was long enough to estimate Attitude Hold pointing errors and vehicle rates. The worst-case RSS attitude error was 15 asec, and the maximum RSS rate was 2.6 asec/sec. T2G worst-case attitude errors were all within the required FGS search radius of 55 asec, and the maximum T2G rates were within the capture range of the FGS. Based upon these simulated results, T2G performance was within requirements and ready to be tested on-orbit.

T2G On-Orbit Performance

The capabilities of the T2G control mode have been successfully demonstrated in-flight. T2G Rate Damping and Attitude Hold performance are shown in Figure 14. T2G effectiveness in damping residual M2G vehicle rates was confirmed over the first 120-days of TGS operation, and the maximum observed M2G rate was 0.014 deg/sec RSS. Rate damping times averaged 8.4 sec, and rate damping was achieved in all cases within the allotted time of 120 sec. Quantization of the flight telemetry channels used to evaluate T2G rate damping times is evident in Figure 14. The primary FGS Spiral Search radius is a good measure of T2G Attitude Hold performance after completion of OBAD correction maneuvers, and search radii are plotted in Figure 14 for more than 10,200 guide star acquisitions over 33-months of TGS operations. Attitude Hold errors averaged 10.0 asec, and the maximum observed search radius, 58.3 asec, is slightly higher than the required 55 asec. T2G has proven to be successful in bridging the M2G and F2G control modes.

FGS AND TWO-GYRO CONTROL MODE (F2G)

The F2G control system design is nearly identical to the T2G control system described earlier and shown in Figure 7, but there are a few differences. The FGS is a low-noise sensor, and filtering of the Gx-axis rate estimate is not required for F2G. The Gyro Bias Observer is used only with the FGS, and the input to the observer is the same Filtered FGS Attitude Error signal presently used in the baseline 3-gyro controller. The F2G control laws are the first to use the full capabilities of the FGS as a rate sensor.

F2G Coarse Track Design

F2G rate control of the Gx-axis begins with the F2G-CT control law, after the primary FGS has acquired its target guide star in Coarse Track. The purpose of this controller is to damp T2G rates so that the primary FGS can successfully acquire its guide star in Fine Lock. The time spent in F2G-CT control is intentionally brief, less than 1-minute, so as not to exacerbate FGS SSS bearing wear by excessive Coarse Track usage. No science imaging is performed during F2G-CT.

The FGS star vector while in Coarse Track is computed based upon Figure 9. The center of the FGS IFOV lies at the tip of the star unit vector in FGS frame, $\bar{s}^F$, which is offset from the HST boresight by angle ρ'/G_{opt}, where G_{opt} is the FGS optical gain. The star vector is computed from SSS angle measurements, θ_A and θ_B, for servos A and B, respectively. The servo angles used for the star vector computation in F2G-CT specify the location of the Coarse Track nutation center, rather than the IFOV

center that is cycling around the light centroid of the guide star. Lever arm angles, δ_A and δ_B, are database constants that are calibrated on-orbit.

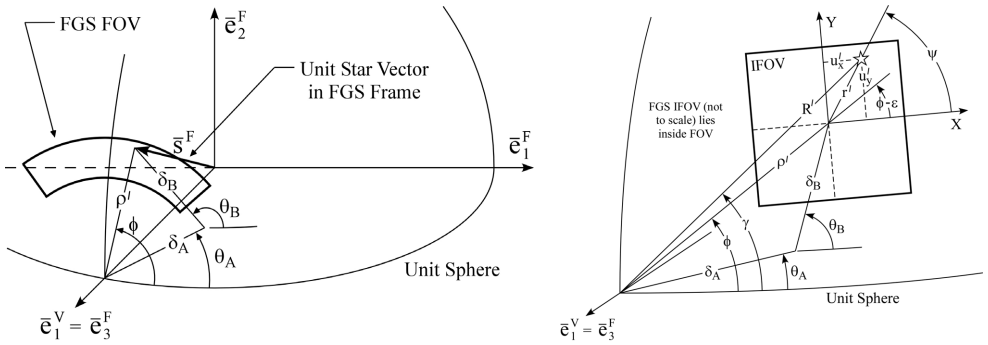

Figure 9 FGS FOV, IFOV, and Star Vector Geometry

The non-linear spherical trigonometric equations for the FGS star vector were never required using the baseline 3-gyro control system, but these equations are now needed to achieve the accuracy required for F2G rate measurement at 40 Hz. The Coarse Track star vector in FGS frame, Eq. (11), is corrected for optical distortion and misalignment and then transformed into the HST vehicle frame prior to use in Eq. (9), the Gx-axis rate estimation equation.

$$\bar{s}^F = \begin{bmatrix} \cos\rho \\ \sin\rho\cos\phi \\ \sin\rho\sin\phi \end{bmatrix} \qquad \begin{aligned} &\rho = \rho'/G_{opt}\,, \quad \rho' = \cos^{-1}\left[\cos\delta_A\cos\delta_B - \sin\delta_A\sin\delta_B\cos\left(\theta_B - \theta_A\right)\right] \\ &\phi = \theta_A + \cos^{-1}\left[\left(\cos\delta_B - \cos\delta_A\cos\rho'\right)/\sin\delta_A\sin\rho'\right], \quad G_{opt} = 57.3 \end{aligned} \tag{11}$$

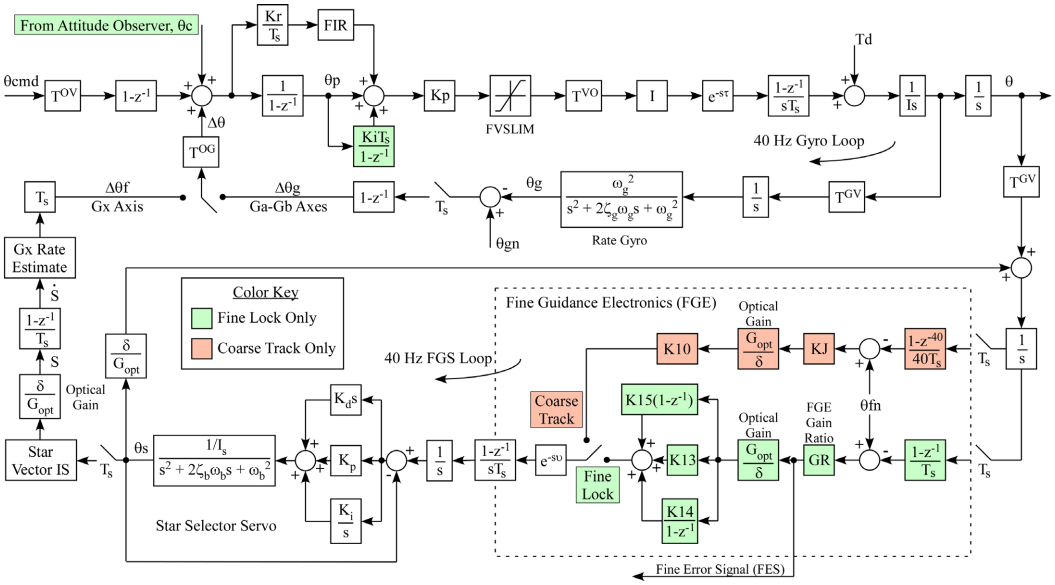

Figure 10 F2G Control Law Block Diagram used for Linear Stability Analysis

The F2G-CT control law block diagram used for linear stability analysis is shown in Figure 10. This control law is a proportional-derivative law, as the control law integral gain and the attitude observer are not used during this brief transition mode that bridges T2G and the F2G Fine Lock submode. Unique to

FGE computation in Coarse Track is the FGE position correction performed at 40 Hz using the current error measurement and a 40-sample-old measurement, as shown in the lower right portion of the figure. In this way, the FGE computes an error correction based upon the current measurement and the measurement the last time the IFOV was at the same location on the Coarse Track nutation circle. Also within the FGE control law is the Coarse Track gain, the K-Factor KJ, which is a function of guide star magnitude. This gain was optimized for F2G-CT to ensure that worst-case T2G rates will damp within 20 sec, and this result was verified using HSTSIM. Note that the portions of the block diagram used only in Coarse Track are shaded red.

F2G-CT stability analysis plots are shown in Figure 11 based upon the block diagram in Figure 10. These are the single-axis linear open-loop transfer function plots for the Gyro Plane axes using the rate gyro sensor and for the Gx-axis using the FGS as a rate sensor. The Gyro Plane plot is identical to the baseline 3-gyro control law Nichols plot, because the TGS Gyro Plane axes use the 3-gyro PD-gains. The F2G-CT Gx-axis has a lower bandwidth (0.11 Hz) than the Gyro Plane axes (1.27 Hz) because of the inherent 1-sec lag in the Coarse Track FGE processing. The Nichols plots indicate adequate stability margins for both the Gyro Plane and Gx-axis controllers in F2G-CT. Control loop stability margins and closed-loop bandwidths are written on the figures. Single-axis stability analysis is sufficient for HST because there is insignificant coupling between OGF axes in F2G mode.

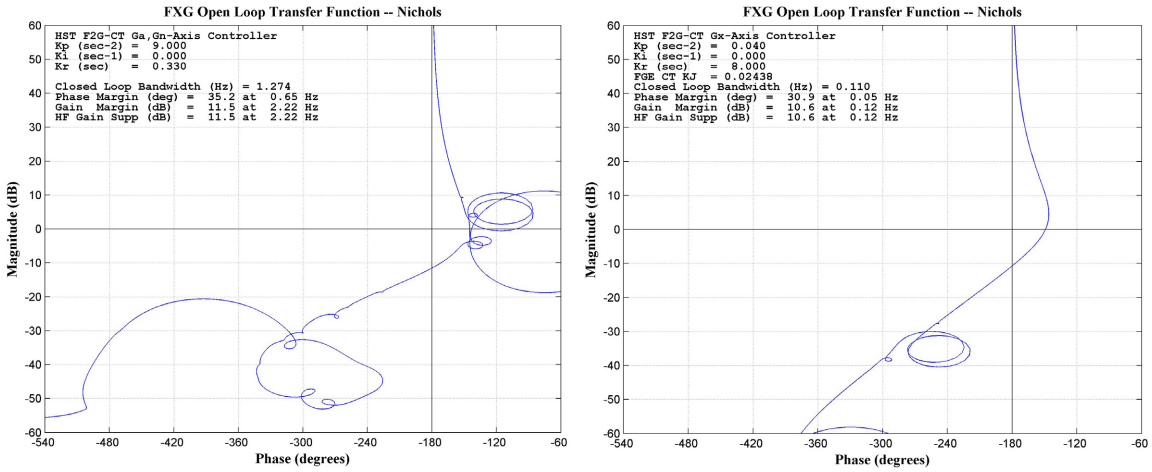

Figure 11 F2G-CT Control Law Nichols Plots for Gyro Plane Axes and Gx-Axis

F2G Fine Lock Design

F2G-FL is the precision pointing control law for Two-Gyro Science. The FGS star vector for Fine Lock is based upon Figure 9, but additional complexity, not used for Coarse Track, is added that specifies the position of the guide star relative to the center of the IFOV. The Fine Lock star unit vector in FGS frame, Eq. (12), is computed at 40 Hz, corrected for optical distortion and misalignment, and transformed into the HST vehicle frame prior to use in Eq. (9), the Gx-axis rate estimation equation. Variables R and γ are computed using Eqs. (11, 13-15). The FGS interferometer Fine Error Signal, or FES, components are computed from PMT counts (A_x, B_x, A_y, B_y) and K-Factor gains in Eq. (15).

$$\bar{s}^F = \begin{bmatrix} \cos R \\ \sin R \cos\gamma \\ \sin R \sin\gamma \end{bmatrix} \qquad \begin{aligned} R &= R'/G_{opt}\,, \quad R' = \rho' + r'\cos(\psi + \varepsilon - \phi) \\ \gamma &= \phi + \left[\sin r' \sin(\psi + \varepsilon - \phi)/\sin\rho'\right] \end{aligned} \tag{12}$$

$$\varepsilon = \phi - \theta_B + \cos^{-1}\left[\cos(\phi - \theta_A)\cos(\theta_B - \theta_A) + \sin(\phi - \theta_A)\sin(\theta_B - \theta_A)\cos\delta_A\right] \tag{13}$$

$$r' = \sqrt{\left(u_x'\right)^2 + \left(u_y'\right)^2} \qquad \psi = \tan^{-1}\left(u_y' \big/ u_x'\right) \tag{14}$$

$$u_x' = K0_x + K1_x\left[\left(A_x - B_x\right)\big/\left(A_x + B_x\right)\right] \qquad u_y' = K0_y + K1_y\left[\left(A_y - B_y\right)\big/\left(A_y + B_y\right)\right] \tag{15}$$

The F2G-FL control law block diagram used for linear stability analysis was shown previously in Figure 10. F2G-FL control uses a proportional-integral-derivative law, and input from the attitude observer is used. The attitude observer used for F2G-FL is identical to the observer used in 3-gyro mode. The FGE control law in Fine Lock uses the Fine Error Signal to drive the Star Selector Servos to center the guide star in the IFOV. Portions of the block diagram used only in Fine Lock are shaded green.

F2G-FL stability analysis plots are shown in Figure 12. The Nichols plots for the Gyro Plane axes are nearly identical to those shown in Figure 11 except for the low-frequency roll-off provided by the F2G-FL integral gain. Using the FGS in Fine Lock as the rate sensor for the Gx-axis, the Nichols plot in Figure 12 shows adequate stability margins and a closed-loop bandwidth of 1.05 Hz, slightly below the bandwidth of the Gyro Plane axes at 1.27 Hz.

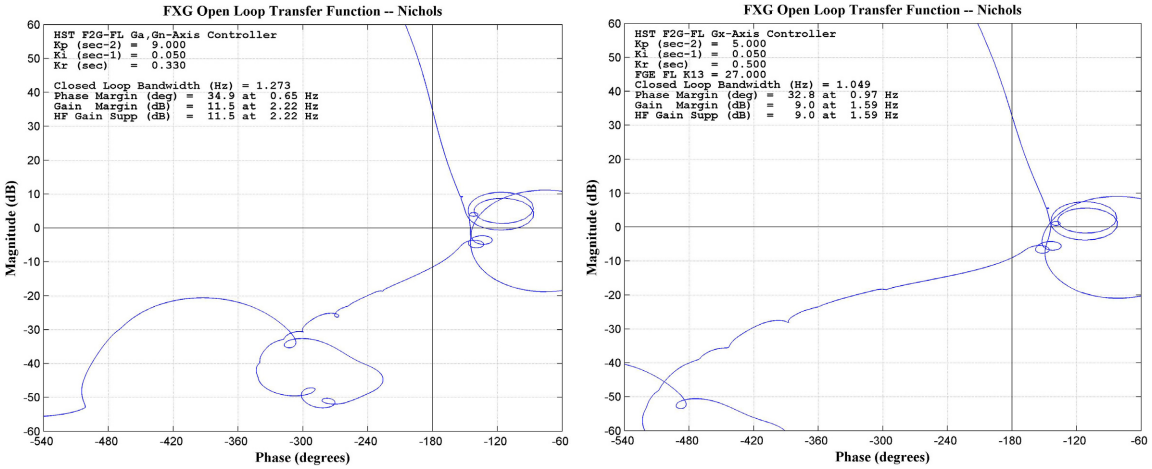

Figure 12 F2G-FL Control Law Nichols Plots for Gyro Plane Axes and Gx-Axis

PCS engineers predicted HST on-orbit pointing stability in F2G-FL by performing time-domain simulations using HSTSIM, and the results are shown in Table 7. With an FGS controlling Gx-axis rate in TGS, HST boresight jitter becomes a function of the dominant FGS guide star magnitude. Faint guide stars produced slightly higher boresight jitter compared with bright guide stars in F2G; however, these simulation results indicated that HST would still meet the 7 mas (1-σ over 60 sec) pointing stability requirement in F2G.

Table 7 HST Pointing Stability in F2G Predicted by HSTSIM

Gyro-A	Gyro-B	Angle between Gx and e_1^V	F2G-FL Boresight Jitter (mas, 60-sec RMS) Versus Dominant Guide Star Magnitude			
			9.0 mv	12.0 mv	13.5 mv	14.5 mv
1	2	90.0°	1.536	2.087	3.124	4.064
1	4	58.0°	1.585	2.010	3.306	4.411
1	6	58.0°	1.586	2.169	3.367	4.473
2	4	36.8°	2.742	2.942	3.688	4.670
2	6	36.8°	2.798	2.986	3.877	4.893
4	6	48.1°	1.903	2.123	3.278	4.355

Numerous simulations were run to demonstrate F2G performance during the design phase prior to on-orbit testing, such as Fine Lock science maneuvers, attitude observer settling, and end-to-end simulations exercising all new TGS modes. The F2G disturbance rejection capability was demonstrated by simulating the affect of known HST thermal-mechanical disturbances caused by SA3, the Optical Telescope Assembly Equipment Shelf (the FHST and rate gyro mounting platform), and the Support System Module. HSTSIM simulations verified a robust F2G design capable of maintaining FGS interferometer lock during these stick-slip thermal-mechanical disturbances.

Under reduced-gyro control, fine-rate sensing is not available in a vector component of the HST boresight axes during the Fine Lock Walkdown, resulting in open-loop drift that can lead to primary FGS guide star acquisition failure. The Gx-axis open-loop portion of the acquisition process is shown in Figure 6. PCS engineers analyzed all environmental torques acting upon the spacecraft to quantify uncompensated disturbances greater than 0.002 Nm resulting in open-loop drift errors during the Walkdown. Refinements were made for on-board modeling of aerodynamic torque compensation and the spacecraft inertia tensor, leading to an improved gravity gradient torque compensation model. The analysis showed that additional feed-forward compensation to counteract solar pressure torques and the dynamic motion of the High Gain Antennas would reduce open-loop drift errors. FGE K-Factors governing the length and speed of the Fine Lock Walkdown were optimized to decrease the duration of the Walkdown time interval. With these changes in place, PCS engineers predicted the probability of primary FGS guide star acquisition success for F2G to be 96.1%, and the success percentage drops to 94.9% in 2009 when the next solar cycle begins to peak.

F2G On-Orbit Performance

TGS has been the nominal pointing control system for the past 33-months, and the success of F2G is proven by HST science images. Figure 13 compares HST images taken with the Advanced Camera for Surveys (ACS), while guiding with 13 mv guide stars, which demonstrates no difference in image quality using the baseline 3-gyro control law and the TGS control law. Note that the images use a logarithmic stretch, which is why the stars have "halos" around them. The stretch was chosen to emphasize the low level contributions of telescope jitter and the outer wings of the point spread function. Geometric distortion and cosmic rays have not been removed from the images. These and many other science images verify that HST pointing stability in F2G is not degraded compared to performance under 3-gyro control.

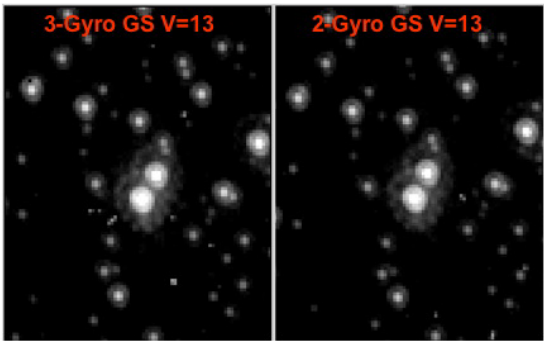

Figure 13 ACS/HRC 555W Logarithmically-Stretched Images (100 sec exposure) Comparing Baseline 3-Gyro Control and TGS Control [Credit: STScI Advanced Camera for Surveys Team]

F2G-FL on-orbit pointing stability is shown in Figure 15 during many science intervals using the baseline 3-gyro control law and TGS for two different gyro pairs (Gyros 1-2 and Gyros 1-6). The figure also overlays polynomial fits for HSTSIM predicted jitter levels. Note that the polynomial curve fits differ slightly from the exact HSTSIM predictions found in Tables 7 and 9. Figure 15 shows that TGS jitter performance varies with dominant guide star magnitude, as expected, and TGS pointing stability is generally better than 3-gyro performance using Gyros 1-2-4. TGS jitter using faint guide stars is similar to 3-gyro jitter, and jitter with the baseline 3-gyro control law is independent of FGS guide star magnitude. Figure 15 shows that TGS jitter using the Gyro 1-2 pair is lower than HST boresight jitter using the Gyro 1-

6 pair, as expected. Finally, on-orbit jitter is approximately 1.5 mas higher than HSTSIM predictions because of nearly persistent low-level disturbances caused by articulation of the High Gain Antenna gimbals.

Other aspects of F2G have proven to be successful on-orbit. FGS guide star acquisition success rates during the open-loop Fine Lock Walkdown were better than 99.2% during the first 15-months on-orbit, exceeding the predicted success rate of 96.1%. The F2G-CT submode has demonstrated successful transitions from T2G by damping initial rates within 4.6 sec on average. The longest observed F2G-CT rate damping time was 18 sec compared to the maximum prediction of 20 sec from HSTSIM.

ONE-GYRO SCIENCE

OGS development for the star-sensing control modes was a straight-forward extension of algorithms and processes already developed for TGS. Both the FHST and the FGS measure two degrees-of-freedom of star position, and the addition of a single gyro provides the minimum number of sensor measurements necessary to successfully control HST rates. The Orthogonal Gyro Frame definition for OGS is different than that used for TGS, and two components of rate are estimated for OGS using the same FHST and FGS star vector equations, Eqs. (10-12), developed for TGS. The T1G and F1G control law structure is nearly identical to the TGS structure shown in Figure 7, except that two components of vehicle rate are computed from star position measurement. TGS control law gains for the Gyro Plane axes are used for the OGS Ga-axis, and TGS Gx-axis gains are used for the OGS gyroless axes, Gn and Gx. The FHST star acquisition process in Figure 5 and the FGS guide star acquisition process in Figure 6 are used without change in OGS. Unfortunately, the M2G design could not be extended into OGS, and the M1G design required a substantial effort to develop a Kalman Filter for HST. The M2G design relied upon simultaneous measurement of vehicle attitude and rate, six degrees-of-freedom, and these were provided by two gyros, two attitude measurements from the Earth magnetic field vector, and the derivative of the magnetic field vector provided Gx-axis rate and attitude rotation about the magnetic field vector. Eliminating one gyro measurement meant that a Kalman Filter was needed to estimate missing measurement information. The OGS feasibility study began in 2004, and the PCS design effort was completed in March 2006. The OGS On-Orbit Test occurred in January 2008 using Gyro-1 in the PCS.

Orthogonal Gyro Frame for One-Gyro Science

The OGF definition for OGS is slightly different from TGS, as shown in Figure 4. The input axis of the gyro used for OGS, the Ga-axis, is normal to the Gyroless Plane, formed by the Gn-axis and Gx-axis. The Gx-axis is defined to be normal to the Ga-axis and the HST boresight axis, $\overline{e}_1^V$, as described in Eq. (16). The definition for the Gn-axis, Eq. (4), also applies for OGS to complete the OGF basis vector set. The transformation matrix, $T_{\alpha\beta}^{OV}$, from the HST vehicle frame to the OGF is computed using Eq. (5).

$$\overline{x}^V = x_1^V \overline{e}_1^V + x_2^V \overline{e}_2^V + x_3^V \overline{e}_3^V = \left(\overline{a}^V \times \overline{e}_1^V\right) \Big/ \left\| \overline{a}^V \times \overline{e}_1^V \right\| \tag{16}$$

A qualitative estimate indicates that OGS pointing stability will be independent of the gyro used in F1G. The angle between the Gyroless Plane and the HST boresight is roughly the same for all possible gyros, as shown in Table 8. However, the same is not true for T1G. Some gyro and FHST combinations result in small angles, less than 15 deg, and T1G pointing errors are expected to be higher for those sensors used for T1G control.

Rate Estimation for Star Sensing Modes in One-Gyro Science

Optimal Gn-axis and Gx-axis rate estimation for T1G and F1G modes is evaluated using the same parameter optimization method used for TGS. For OGS, it is convenient to transform the FHST or FGS star vector measurement, $\overline{s}^V$, from the HST vehicle frame into the OGF. The same star vector equations used for TGS, Eqs. (10-12), are used for OGS. The total derivative of the star vector in the OGF is given by Eq. (17) after introducing a nominally zero error vector, $\overline{\lambda}^O$, and inserting expressions found in Eq. (7). Minimizing the cost function, J, in Eq. (18) with respect to the unknown Gn-axis and Gx-axis vehicle

rates, ω_2^O and ω_3^O, results in the OGS rate estimation equations, Eq. (19). Computation of OGS star vector derivatives follows the same rules developed for TGS.

$$\overset{o}{\bar{s}}{}^O = \dot{\bar{s}}^O + \bar{\omega}^O \times \bar{s}^O \qquad \bar{\lambda}^O = \overset{o}{\bar{s}}{}^O - \dot{\bar{s}}^O + \bar{\tilde{s}}^O \bullet \bar{\omega}^O \qquad \bar{\tilde{s}}^O = \bar{\bar{T}}^{OV} \bullet \bar{\tilde{s}}^V \tag{17}$$

$$\frac{\partial J}{\partial \omega_2^O} = 0 \qquad \frac{\partial J}{\partial \omega_3^O} = 0 \qquad J = \sum_{\alpha=1}^{3} \left(\lambda_\alpha^O\right)^2 \tag{18}$$

$$\omega_2^O = -\sum_{\alpha=1}^{3}\sum_{\beta=1}^{3} \tilde{s}_{3\alpha}^O \tilde{s}_{\alpha\beta}^O \left(\dot{s}_\beta^O - \overset{o}{s}{}_\beta^O - \tilde{s}_{\beta 1}^O \omega_1^O\right) \Big/ s_1^O \qquad \omega_3^O = \sum_{\alpha=1}^{3}\sum_{\beta=1}^{3} \tilde{s}_{2\alpha}^O \tilde{s}_{\alpha\beta}^O \left(\dot{s}_\beta^O - \overset{o}{s}{}_\beta^O - \tilde{s}_{\beta 1}^O \omega_1^O\right) \Big/ s_1^O \tag{19}$$

Table 8 Angles between Gyroless Plane and HST and FHST Boresights for Gyros in OGS

Gyro	FHST	Gn (V1-Axis)	Gn (V2-Axis)	Gn (V3-Axis)	Gx (V1-Axis)	Gx (V2-Axis)	Gx (V3-Axis)	Angle Between Gyroless Plane and V1 (degrees)	Angle Between Gyroless Plane and FHST Boresight (degrees)
1	1	0.851	0.000	-0.526	0.000	-1.000	0.000	31.700	58.300
1	2	0.851	0.000	-0.526	0.000	-1.000	0.000	31.700	64.287 &
1	3	0.851	0.000	-0.526	0.000	-1.000	0.000	31.700	64.287 &
2	1	0.851	0.000	0.526	0.000	1.000	0.000	31.700	58.300
2	2	0.851	0.000	0.526	0.000	1.000	0.000	31.700	12.291 +
2	3	0.851	0.000	0.526	0.000	1.000	0.000	31.700	12.291 +
3	1	0.811	-0.446	-0.380	0.000	-0.648	0.761	35.850	31.700
3	2	0.811	-0.446	-0.380	0.000	-0.648	0.761	35.850	73.876 &
3	3	0.811	-0.446	-0.380	0.000	-0.648	0.761	35.850	29.616
4	1	0.811	-0.446	0.380	0.000	-0.648	-0.761	35.850	31.700
4	2	0.811	-0.446	0.380	0.000	-0.648	-0.761	35.850	15.827
4	3	0.811	-0.446	0.380	0.000	-0.648	-0.761	35.850	11.172 +
5	1	0.811	0.446	-0.380	0.000	-0.648	-0.761	35.850	31.700
5	2	0.811	0.446	-0.380	0.000	-0.648	-0.761	35.850	29.616
5	3	0.811	0.446	-0.380	0.000	-0.648	-0.761	35.850	73.876 &
6	1	0.811	0.446	0.380	0.000	-0.648	0.761	35.850	31.700
6	2	0.811	0.446	0.380	0.000	-0.648	0.761	35.850	11.172 +
6	3	0.811	0.446	0.380	0.000	-0.648	0.761	35.850	15.827

& Best T1G | + Worst T1G

TRACKER AND ONE-GYRO CONTROL MODE (T1G)

As designed and tested, T1G incorporates two minor modifications relative to T2G. In order to meet T1G Rate Damping duration goals in all cases, a rate estimate extrapolation capability was added for T1G. If T1G Rate Damping control is open loop about the gyroless axes because no settled rate estimates are available from the FHSTs and the last-available Gn-Gx rate estimates were higher than a database-defined threshold, then those last-available Gn-Gx rate estimates will be extrapolated based on commanded torques, and the extrapolated rate estimate will be used in the T1G control law. This open-loop extrapolation ensures that the rate damping duration timer will not expire without control effort being applied because of the open-loop condition. The second design change relative to T2G also pertains to the Rate Damping submode. As designed and tested on-orbit, the T1G Rate Damping duration was set to 120 sec to ensure that vehicle rates up to 0.03 deg/sec about Gn and Gx would be arrested prior to transition to the Attitude Hold gains and limits. OGS OOT results indicated significantly lower initial rates in T1G-RD at transition from M1G, and the T1G rate damping timer will be reduced to match the T2G value of 60 sec for future OGS operations. This parameter will be revised as predicted worst-case M1G rates change, for example, as aerodynamic torques increase due to higher average atmospheric density at peaks in the solar cycle.

The T1G design was evaluated using HSTSIM to demonstrate robust performance under stress conditions. The T1G Rate Damping submode was presented with more than twice the worst-case expected initial rates about each gyroless axis (0.08 deg/sec) to determine worst-case rate damping time. The longest time required to reduce total true body rates below 2 asec/sec was 121 sec, so in practice, 120 sec was regarded as a very conservative value for the Rate Damping timer. The T1G Maneuver submode was tested by simulating 15° and 0.5° maneuvers, and the worst-case attitude errors following the maneuvers were 89 asec and 15 asec, respectively. The Attitude Hold submode was simulated to determine peak attitude and rate errors over long-duration intervals. The worst-case RSS attitude error was 25 asec, and the

worst-case RSS rate error was 2.8 asec/sec. As expected, the worst case attitude and rate errors were found in OGS configurations with the smallest separation between the Gyroless Plane and the rate control FHST boresight, e.g. FHST-2 with Gyro-2, as shown in Table 8. Based on these results and operational experience with the very similar T2G mode, the T1G mode was regarded as validated and ready for on-orbit test.

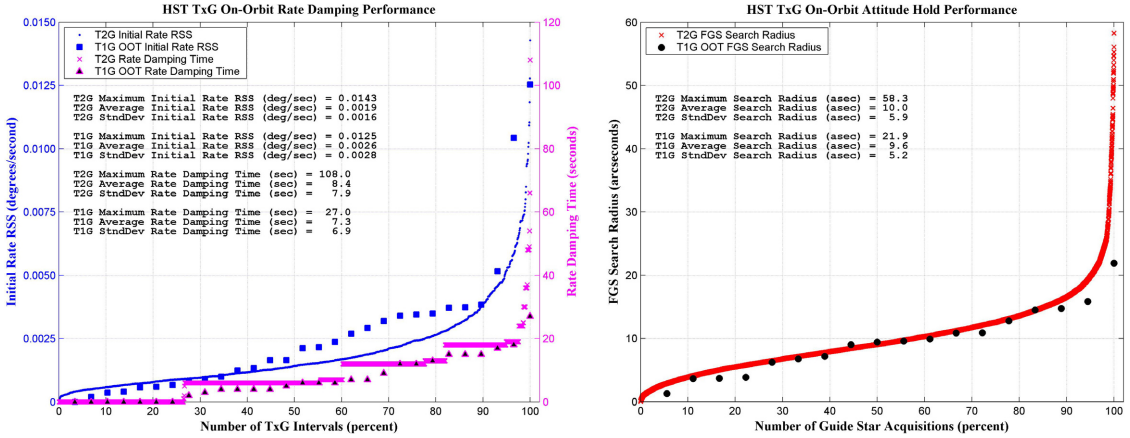

Figure 14 TxG On-Orbit Rate Damping and Attitude Hold Performance

The OGS OOT performance of the T1G Rate Damping submode was assessed by determining initial Gn and Gx-axis RSS rate estimates and the time required to reduce the initial rates below the noise level. The maximum time required to damp initial rates in T1G during the on-orbit test was 27 sec, and the peak Gn and Gx-axis RSS rate at Rate Damping start was 0.0125 deg/sec, as indicated in Figure 14. A combined measure of T1G Attitude Hold, OBAD, and maneuver performance is provided by the primary FGS search radii during guide star acquisitions. This is a measure of residual pointing error after the second OBAD maneuver correction plus any pointing error that is incurred during T1G Attitude Hold after the second OBAD and prior to the guide star acquisition search. A plot of the FGS search radii from the OGS OOT is shown in Figure 14. The maximum search radius was 22 asec, well within the design goal of 55 asec, so the measured FGS search radii indicate very good T1G Attitude Hold performance on-orbit.

FGS AND ONE-GYRO CONTROL MODE (F1G)

The F1G controller required three minor database and gain changes relative to the F2G design to meet science performance goals. To damp worst-case T1G rates in F1G-CT, the rate damping timer increased from 20 sec, used in F2G-CT, to 25 sec. The additional time in F1G-CT increased the overall Coarse Track time for the primary FGS to 34 sec in OGS. The FGE Control Law position gain K-Factor, K13, was increased 25% to improve disturbance rejection for the F1G-FL control law, during thermal-mechanical SA3 disturbance events, at the expense of less than 0.2 mas of additional boresight jitter. The K13 gain is shown in Figure 10. Linear analysis of both the FGE and F1G-FL control laws showed adequate stability margins with this gain increase. The final change for F1G was to activate the Fine Error Signal, Eq. (15), in the star vector computation. HSTSIM simulations predicted that the FES provided the F1G-FL control system with increased rejection of thermal-mechanical disturbances. The F2G implementation zeroed the FES to reduce FGS star vector noise.

HSTSIM was used to predict many aspects of F1G performance for Coarse Track and Fine Lock operations. F1G-CT simulations focused upon the time to damp residual T1G rates. While simulations showed rare cases (less than 1%) where acquisition would fail due to an unacceptably long settling time, the large majority of cases successfully damped the T1G residual rate within the required 25 sec. F1G-FL simulations focused upon pointing performance during normal operations and through a series of known on-orbit disturbances that are modeled in HSTSIM. The performance metrics included boresight jitter estimates and the ability to maintain interferometer lock. Modeled disturbances included persistent disturbances due to High Gain Antenna ephemeris tracking, larger single-event disturbances due to HGA

spline maneuvers, and thermal-mechanical SA3 and Support System Module disturbances. HSTSIM predictions for F1G-FL quiescent pointing stability are listed in Table 9. Comparing these results with simulated F2G performance (in Table 7) shows that boresight jitter is slightly higher with the F1G controller, but the predicted jitter is within the 7 mas HST pointing stability requirement. F1G-FL jitter also shows a similar dependency upon guide star magnitude that was observed in F2G-FL. F1G probability of guide star acquisition success during the open-loop Fine Lock Walkdown interval was predicted to be better than 94.4%, slightly lower that the F2G estimate, in 2009 when the next solar cycle begins to peak.

Table 9 HST Pointing Stability in F1G Predicted by HSTSIM

Gyro	Angle Between Gyroless Plane and e_1^V	F1G-FL Boresight Jitter (mas, 60-sec RMS) Versus Dominant Guide Star Magnitude			
		9.0 mv	12.0 mv	13.5 mv	14.5 mv
1	31.7°	1.350	2.879	5.080	6.580
2	31.7°	1.551	2.757	4.980	6.699
3	35.9°	1.480	2.790	5.352	6.327
4	35.9°	1.402	2.765	5.440	6.466
5	35.9°	1.432	2.726	5.147	6.511
6	35.9°	1.553	2.560	5.102	6.714

The F1G control mode was verified during the on-orbit test to be a productive science mode through a series of 18 successful guide star acquisitions. During these guiding intervals, the HST was able to acquire the correct guide stars and maintain interferometer lock throughout the guiding interval, while rejecting nominal vehicle disturbances. Science images were successfully obtained throughout all guiding intervals. A key metric of F1G performance is HST pointing stability, which was measured during all Fine Lock guiding intervals. A comparison of on-orbit jitter to dominant guide star magnitude across the three HST science control modes is presented in Figure 15. This comparison illustrates that for the reduced-gyro modes, HST boresight jitter is a function of the dominant guide star magnitude, and jitter increases when using faint guide stars. This result is consistent with simulation predictions. Faint guide stars were deliberately selected during the OGS OOT to demonstrate F1G-FL robustness and to verify worst-case boresight jitter performance. Figure 15 shows excellent agreement comparing HSTSIM predicted jitter with F1G flight performance during the OOT, and the data also illustrates the affect of the FES activation in the F1G star vector computation that increases F1G jitter relative to F2G levels. These data verify the successful on-orbit performance of both TGS and OGS to meet the 7 mas pointing stability requirement and to ensure the same science image quality with one or more gyros functioning in the HST PCS.

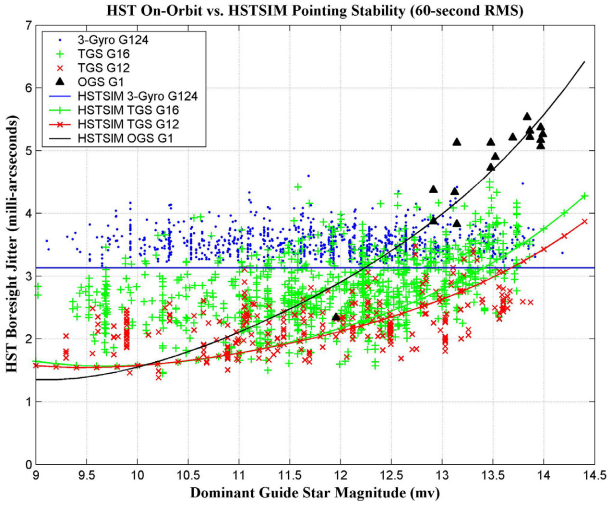

Figure 15 HST On-Orbit Pointing Stability and HSTSIM Predictions vs. Guide Star Magnitude

HST BEYOND 2008

The Hubble Space Telescope has made exceptional discoveries since its launch in 1990 and there is no plan to halt its production of science anytime soon. The current End of Mission (EoM) for the Hubble Space Telescope is planned for no earlier than 2013. Visions of the future of HST include parallel observations with the other Great Observatories to expand the spectrum of discovery.

Servicing Mission 4

In order to continue the historic and successful science mission of the HST throughout its lifetime, NASA has approved SM4 to repair critical components and upgrade HST science capabilities. Launch is currently planned for October 2008 on Space Shuttle Atlantis. The engineering manifest for SM4 includes six new rate gyros, a refurbished FGS, six nickel hydrogen batteries, and new thermal blankets. These repairs will enable the high performance attitude control for which HST is renowned and provide the necessary power for the new generation of scientific instruments. The scientific instrument complement will be upgraded through two new cutting-edge instruments that will enhance the scientific capabilities of the HST. The Cosmic Origins Spectrograph will be the most sensitive ultraviolet spectrograph ever flown on the HST, and the Wide Field Camera 3 will provide a broad-spectral imaging capability over near-ultraviolet through near-infrared wavelengths. Additionally, two current instruments, the Space Telescope Imaging Spectrograph and the Advanced Camera for Surveys, have suffered on-orbit failures and will be repaired. When the upgrades and repairs are complete, these instruments may increase science productivity to new levels, thereby adding to the spectacular history of HST imaging.

Gyro Lifetime Predictions

There are many factors that will determine the final HST EoM. Excluding programmatic factors, hardware failures or orbit degradation are the primary reasons for EoM. It is anticipated that orbit degradation to the science floor will occur approximately 17 years post-SM4. Over HST's 18 year lifespan, there have been few reoccurring hardware failures other than gyro failures. Based on this history, it is prudent to assume that the gyros will be the life limiting hardware asset post-SM4. A gyro management plan consistent with the science floor timeline was developed to maximize science return over the planned lifetime. Through Shuttle servicing of the HST, 16 gyros have flown on the HST giving rise to the possibility of performing a probabilistic gyro lifetime analysis. Based upon observed failure modes, there exist both run-time dependent and run-time independent failure modes that operate independently from each other. To model the different failures, run-time dependent failures are modeled using Weibull Distributions; run-time independent failures are modeled using Exponential Distributions. The total probability function is then calculated from the Laws of Total and Joint Probability. Using a Monte Carlo approach, science return can be computed during the expected gyro lifetimes. For average gyro lifetimes of 5 years, the new set of gyros will last 10 years, on average, if the control mode is limited to 3-gyro operations. By utilizing the reduced-gyro control modes, this lifetime can be significantly extended to 30 years, beyond the time when the science floor altitude is reached. The TGS and OGS control laws have given the HST flexibility to maximize science over a shorter period or to continue reduced-gyro operations after SM4 to obtain an even greater science return over a longer lifetime as program priorities dictate.

CONCLUSION

Reduced-gyro control laws for the Hubble Space Telescope have been designed, implemented, and successfully tested on-orbit. The Two-Gyro Science and One-Gyro Science control laws demonstrate on-orbit boresight pointing stability better than the 7 milli-arcseconds (60-second RMS) required for science imaging. These are the first HST control laws to use star sensors for rate and attitude control, and they achieve on-orbit pointing stability comparable to the performance of the baseline 3-gyro control law. Following coarse-attitude control using magnetometers, TGS and OGS use Fixed Head Star Trackers to damp rates of up to 0.06 degrees/second and correct attitude errors as large as 12 degrees prior to performing science imaging in Fine Lock with milli-arcsecond accuracy using Fine Guidance Sensors. These reduced-gyro control laws have provided the Hubble Space Telescope with an opportunity to continue its science mission well into the future while preserving the science image quality that remains a trademark of the observatory.

ACKNOWLEDGEMENT

The authors wish to acknowledge the efforts of all present and past members of the Pointing Control System and Safing groups who contributed to the development of the HST reduced-gyro control modes: Satyan Anandakrishnan, Brian Clapp, Martin Gakenheimer, Sun Hur-Diaz, Edward Kimmer, Edward Moy, David Murphy, Mike Myslinski, Patrick Ramsey, James Seidel, C. Eugene Skelton, Daniel Smith, John Van Arsdall, and John Wirzburger. We also wish to acknowledge the expertise and guidance provided by our technical peers throughout the TGS and OGS development cycles: Mike Femiano, F. Landis Markley, and Hugh Dougherty. This work was sponsored by the NASA Goddard Space Flight Center, Greenbelt, MD, under Contract NAS5-50000.

NOTATION

Table 10 Vector and Tensor Nomenclature

Symbol	Description
$\overline{a}^A$	Vector $\overline{a}$ written in coordinates of Reference Frame A
a_α^A	Component α of vector $\overline{a}$ in Reference Frame A coordinates
$\overline{e}_\alpha^A$	Component α of unit vector $\overline{e}$ in Reference Frame A coordinates
$\overline{\overline{T}}^{AB}$	Transformation tensor from Frame B to Frame A, equals $\overline{e}_\alpha^A T_{\alpha\beta}^{AB} \overline{e}_\beta^B$ for $(\alpha,\beta = 1,2,3)$
$T_{\alpha\beta}^{AB}$	Transformation matrix element in row α and column β of tensor $\overline{\overline{T}}^{AB}$

REFERENCES

1. H. Dougherty, K. Tompetrini, J. Levinthal, and G. Nurre, "Space Telescope Pointing Control System," *AIAA Journal of Guidance, Control, and Dynamics*, Vol. 5, No. 4, July-August 1982, pp. 403-409.

2. G. A. Beals, R. C. Crum, H. J. Dougherty, D. K. Hegel, J. L. Kelley, and J. J. Rodden, "Hubble Space Telescope Precision Pointing Control System," *AIAA Journal of Guidance, Control, and Dynamics*, Vol. 11, No. 2, March-April 1988, pp. 119-123.

3. D.J. Eaton, R.A. Whittlesey, B.W. Allen, R. Stoll, L. Abramowicz-Reed, and M. Marcel, "On-orbit Performance of the Hubble Space Telescope Fine Guidance Sensors," *Applied Optics*, Vol. 32, No. 10, 1993, p. 1689ff.

4. J.P. Sharkey, G.S. Nurre, G.A. Beals, and J.D. Nelson, "A Chronology of the On-orbit Pointing Control System Changes on the Hubble Space Telescope and Associated Pointing Improvements," *1992 AIAA Technical Papers*, Part 3 (A92-55151 23-63), AIAA-1992-4618, pp. 1418-1433. AIAA Guidance, Navigation and Control Conference, Hilton Head Island, SC, Aug 10-12, 1992.

5. N. Vadlamudi, M.A. Blair, and B.R. Clapp, "Hubble Space Telescope On-orbit Transfer Function Test," *1992 AIAA Technical Papers*, Part 3 (A92-55151 23-63), AIAA-1992-4614, pp. 1409-1417. AIAA Guidance, Navigation and Control Conference, Hilton Head Island, SC, Aug 10-12, 1992.

6. G.S. Nurre, S.J. Anhouse, and S.N. Gullapalli, "Hubble Space Telescope Fine Guidance Sensor Control System," *Acquisition, Tracking, and Pointing III,* SPIE Vol. 1111, 1 September 1989, pp. 327-343.

7. D.A. Nichols, R.P. Headley, and C.P. Bradley, "Dynamic Testing of the CT401 and the Enhanced NASA Standard Star Trackers," *1980 AIAA Technical Papers* (A80-45514 19-17), AIAA-1980-1741, pp. 174-182. AIAA Guidance and Control Conference, Danvers, MA, August 11-13, 1980.

8. C.E. Skelton, S. Hur-Diaz, P.R. Ramsey, J.P. Seidel, D.C. Smith, J.C. Van Arsdall, and J.H. Wirzburger, "Hubble Space Telescope Magnetic Sensing System and Reduced Gyro Control," *AAS F. Landis Markley Astronautics Symposium*, AAS-08-277, June 2008.

9. M. Prior and L. Dunham, "System Design and Performance of the Two-Gyro Science Mode for the Hubble Space Telescope," *56th International Astronautical Congress*, Fukuoka, Japan, October 17-21, 2005.